crystals

MDPI

Article

A Fibrous Perovskite Nanomaterial with Exsolved Ni-Cu Metal Nanoparticles as an Effective Composite Catalyst for External Steam Reforming of Liquid Alcohols

Tong Wei [1,2,*], Juan Wang [1], Yangbo Jia [2] and Tatsukuni Harimoto [1]

[1] Department of Hydrogen Energy, Tianneng Holding Group, 18 Baoqiao Road, Huaxi Street, Huzhou 313100, China; zhangshuguo@tiannenggroup.com (T.H.)
[2] School of Materials Science & Engineering, Zhejiang Sci-Tech University, Hangzhou 310018, China
* Correspondence: weit@zstu.edu.cn

Abstract: The conversion of hydrogen to power via combined external reforming of liquid alcohol and solid oxide fuel cell (SOFC) technology is an effective approach to address future energy challenges. In this study, an $La_{0.8}Ba_{0.1}Mn_{0.8}Ni_{0.1}Cu_{0.1}O_3$ (LBMNCu) perovskite nanofiber with high porosity was synthesized with a modified electrostatic spinning method, which acted as an efficient catalyst for steam reforming of liquid alcohols (methanol and ethanol). After reduction, fine metallic Ni-Cu was uniformly distributed throughout the perovskite nanofiber surface. The obtained composite displayed a methanol conversion above 99.9% at 450 °C and an ethanol conversion above 99% at 600 °C, which was highly superior to the common Ni-Cu/Al_2O_3 catalyst. The catalytic performance of our assembled catalysts also remained stable in methanol and ethanol atmospheres for 50 h and no coking was detected. Furthermore, when the reformed gas was fed into a $Y_{0.08}Zr_{0.92}O_2$ (YSZ)-based SOFC system, the open circuit voltage remained around 1.1 V at 700 °C for 50 h accordingly, without coking, and the voltage remained virtually unchanged at 0.7 V for 50 h at 700 °C and 400 mA cm^{-2} during galvanostatic discharge mode, indicating that using LBMNCu nanofiber as a catalyst for hydrogen production and utilization is an efficient strategy. The interaction of the in situ exsolved metallic nanoparticles and nanofibrous perovskite could also be a promising approach for designing a highly active catalyst for H_2 generation.

Keywords: perovskite nanofiber; metallic Ni-Cu nanoparticles; external steam reforming; methanol and ethanol; solid oxide fuel cells

Citation: Wei, T.; Wang, J.; Jia, Y.; Harimoto, T. A Fibrous Perovskite Nanomaterial with Exsolved Ni-Cu Metal Nanoparticles as an Effective Composite Catalyst for External Steam Reforming of Liquid Alcohols. *Crystals* **2023**, *13*, 1594. https://doi.org/10.3390/cryst13111594

Academic Editor: Vladislav V. Kharton

Received: 30 October 2023
Revised: 13 November 2023
Accepted: 14 November 2023
Published: 17 November 2023

1. Introduction

Hydrogen is expected to become the main source of environmentally friendly clean fuels and energy storage medium in the future. It can be effectively converted into electric energy [1] via fuel cells with low greenhouse gas emissions. Due to the rapid development of fuel cell technology, the development and demand of new methods to produce hydrogen are increasing rapidly. Steam reforming of hydrocarbons, especially CH_4, is a general strategy to produce hydrogen [2], but the high temperature conditions and high energy consumption make it a less than ideal choice. Methanol steam reforming (MSR) and ethanol steam reforming (ESR) can yield a 75% concentration of hydrogen as produced gas (Equations (1) and (2)), accompanied with the side reactions (Equations (3) and (4)), which involve CO generation under the effect of various catalysts and reaction conditions [3,4].

$$CH_3OH(g) + H_2O(g) \rightarrow 3H_2 + CO_2 \quad (1)$$

$$C_2H_5OH(g) + 3H_2O(g) \rightarrow 6H_2 + 2CO_2 \quad (2)$$

$$H_2 + CO_2 \rightarrow CO + H_2O(g) \quad (3)$$

$$CH_3OH(g) \rightarrow 2H_2 + CO \quad (4)$$

Here, methanol and ethanol can be considered as hydrogen carriers and hydrogen would be produced when using it. Based on the convenient transportation of liquid alcohols, MSR and ESR can provide a new mode of realizing hydrogen production and utilization [5]. Considering that solid oxide fuel cells (SOFC) operate at high temperatures (above 600 °C) and the non-precious Ni-based anode displays better resistance to CO [6,7], the conversion of hydrogen to power via combination of steam reforming and SOFC technology is an effective and promising approach to address future energy challenges.

However, ethanol decomposition and dehydrogenation would also produce carbon deposition on the surface of catalysts, which challenges the catalytic performance. Ideally, the catalyst should be highly active for H_2 production with excellent stability.

Precious metals (Pt, Rh, etc.) are usually loaded on metal oxide substrates, such as Al_2O_3, SiO_2, CeO_2 and ZrO_2, and are used as catalysts for ESR, showing good H_2 selectivity and high coking resistance [8–10]. Considering the cost, non-precious metals such as Ni, Cu, Co and Fe are usually preferred as active elements. Among them, the Cu-based catalysts have been widely studied for MSR because of their high activity and selectivity. Ni is also widely used and shows high catalytic activity in C-C and O-H bond breaking, promoting hydrogen formation by H atoms and enhancing selectivity [11,12]. However, Cu would suffer deactivation due to sintering and Ni because of carbon deposition.

Perovskite oxide is a kind of novel inorganic non-metallic material with unique physical and chemical properties. Many studies have found that ABO_3-type perovskite oxide has the advantages of controllable structure, good thermal stability, high catalytic efficiency and low price, and has been widely used in reforming reactions [13–15]. It can be used as a precursor to assemble fine metallic nanoparticles separated on the surface of the perovskite substrate, with stronger metal support interaction and more satisfactory anti-sintering ability than the impregnation method, which is also called in situ exsolution technology [16–18]. In addition, the A-site-deficient perovskites ($A/B < 1$) employed could promote B-site metallic element exsolution [19,20], as the A-site deficiency provides a driving force for reduction of the doped metal, which is shown in Equation (5):

$$A_{1-\alpha}BO_{3-\delta} \rightarrow (1-\alpha)ABO_{3-\gamma} + \alpha B \quad (5)$$

The perovskite oxide precursor is commonly prepared by a traditional powder synthesis method such as sol-gel and solid-reaction process and displays a relatively lower specific surface area, which limits the amount of active site and catalytic performance, as well as the application. Recently, more and more researchers have paid attention to the morphologic design to further improve the catalytic performance of perovskite catalysts through the modification of pore-size distribution, surface area and microstructure [21,22]. Among these methods, a facile electrospinning method has been proven to produce catalysts with an unusually porous nanotube structure [23,24].

In order to produce bi-metallic nanoparticles supported on a porous perovskite oxide substrate to serve as a highly efficient catalyst for the MSR/ESR, an electrostatic spinning method was introduced to improve the porous structure and surface area of the traditional perovskite oxides, thus further increasing the number of active sites and enhancing catalytic performance. The A-site deficiency was expected to promote the exsolution of the metallic Ni-Cu after reduction on the substrate of the LBMNCu.

In this case, a $La_{0.8}Ba_{0.1}Mn_{0.8}Ni_{0.1}Cu_{0.1}O_3$ (LBMNCu) perovskite nanofiber with high porosity was synthesized with a modified electrostatic spinning method, which acted as an efficient catalyst for steam reforming of methanol and ethanol for the first time. To verify the advantage of the assembled catalyst, the LBMNCu perovskite powder as well as the general reforming catalyst, Ni-Cu/Al_2O_3, were also prepared and the catalytic performance was also investigated for comparison. For evaluating the practical application of external

reforming, the reformed gas was fed into SOFCs directly and the voltage was recorded simultaneously under a galvanostatic discharge mode.

2. Materials and Methods

2.1. Materials Preparation

The LBMNCu fibers were synthesized via electrospinning method, in which $La(NO_3)_3{\cdot}6H_2O$, $Ba(NO_3)_2$, $Mn(NO_3)_2$, $Ni(NO_3)_2{\cdot}6H_2O$ and $Cu(NO_3)_2{\cdot}H_2O$ with a La/Ba/Mn/Ni/Cu molar ratio of 8:1:8:1:1 mixed with polyvinylpyrrolidone (PVP) were all dissolved into N, N-dimethylformamide (DMF) and the resulting solution was fed into a 20 mL plastic syringe equipped with a 22-gauge stainless steel nozzle on the spinning instrument. The operating voltage was set as 20 kV and the distance between the collector and the needle tip was 20 cm. The collected electrospun nanofibers were subsequently calcined at 700 °C for 3 h in air to obtain the LBMNCu nanotubes. LBMNCu powders were also prepared by an optimized sol-gel technique. In a typical process, $La(NO_3)_3{\cdot}6H_2O$, $Mn(NO_3)_2{\cdot}4H_2O$, $Ba(NO_3)_2$, $Ni(CH_3COO)_2{\cdot}4H_2O$ and $Cu(NO_3)_2{\cdot}H_2O$ were totally dissolved into deionized water. Subsequently, citric acid was added as the complexing agent with a molar ratio 1.5 times that of total metal cations, and ammonia aqueous solution was added to adjust the pH value to 8. The aqueous solution was stirred at 80 °C until a sticky gel was formed, and then the obtained gel was dried in an oven at 200 °C. Subsequently, the obtained powder was ground and calcined at 1000 °C for 3 h to form LBMNCu nanoparticles. To understand Ni exsolution in LBMNCu in reducing atmosphere, the prepared LBMNCu nanoparticles and nanofibers were reduced in a 10% H_2-N_2 stream at 600 °C for 3 h. The Ni-Cu/Al_2O_3 was prepared by submerging g-Al_2O_3 powder into an aqueous $Ni(NO_3)_2{\cdot}6H_2O$ and $Cu(NO_3)_2{\cdot}H_2O$ solution with equal metal ion ratio under stirring at 80 °C to evaporate water. The dried powder was heated subsequently at 400 °C for 3 h, and then reduced in a 10% H_2-N_2 stream at 300 °C for 2 h. The total metal loading on the g-Al_2O_3 powder was 20 wt.% for all combinations.

2.2. Characterization

The X-ray diffractometer (D8/A8 Advance, Bruker AXS, Beijing, China) was used for physical phase analysis of the material with a Cu kα radiation (1.5405 Å) with a scanning angle range of 20–80° and a scanning speed of 5° min^{-1}. The porous structure of the catalyst was characterized by the N_2 adsorption/desorption (BET) method using an ASAP 2460 micropore (Micromeritics, Shanghai, China) analyzer. Prior to characterization, the samples were degassed under vacuum at 200 °C for 10 h. A field emission scanning electron microscope (FE-SEM, Gemini 300, ZEISS, Oberkochen, Germany) was used to observe the microstructure of the powder and bulk materials, including surface morphology, exsolved nanoparticles and carbon deposition of the prepared, reduced and post-test materials as well as the morphology of the fabricated cells and post-test cells. After catalytic testing, the material was examined by a Raman spectrometer (XploRA, Horiba JobinYvon, Paris, France) to determine the presence of carbon.

2.3. Catalytic Test

The catalytic activity of steam methanol/ethanol reforming was evaluated using a 0.5 g catalyst in a fixed bed quartz tube reactor. Prior to each test, the catalyst was reduced in situ at 10%H_2/N_2 flow at 600 °C, the methanol/ethanol solution was added to the evaporator through a liquid injection pump, and then the gas reactant was added to the catalytic reactor. The pipe between the steam generator and the quartz reactor is wrapped with tropical zones to ensure that the methanol water vapor does not condense. For all catalyst experiments in this study, we set the water/methanol mole ratio (W/M) to 1 or 1.2, the flow rate to 4 mL/h, water/ethanol (W/E) to 3 or 3.5 using a precise injection pump. The unreacted condensable species were collected in an ice bath condenser. An online gas chromatograph equipped with a thermal conductivity detector (TCD) and TDX-01 column,

and a flame ionization detector (FID) and Porapak-Q column was used for analysis of the final products including H_2, CO, and CO_2 and unreacted alcohols.

2.4. SOFC Test

The anode-supported cell was prepared by casting strip screen printing and sintering process. Generally, raw powder mixture containing NiO (Inco) and $Y_{0.08}Zr_{0.92}O_2$ (YSZ, TZ-8YS, Tosoh, Shunan, Japan) at a weight ratio of 57:43, was ball-milled for 24 h in a toluene/ethanol mixture solvent, with fish oil as dispersant and corn starch as well-forming agent. The slurry was cast into sheets using a tape casting machine to obtain a dry sheet (1.4 mm thick) as anode support, then printed YSZ electrolyte on the surface screen and sintering in 1390 °C of air for 4 h. To prepare the cathode, the $La_{0.6}Sr_{0.4}Co_{0.2}Fe_{0.8}O_{3-\delta}$ (LSCF)-YSZ (70:30) slurry was printed on the surface of the sintered YSZ electrolyte and sintering in 900 °C of air for 3 h to complete the manufacture of the anode support cell.

For electrochemical performance measurement, the four-electrode method was used to test the performance of a single cell to effectively eliminate the influence of the ohm resistance of the collector wire, in which two Pt lines are connected to the positive and negative extremes. After assembly and sealing, H_2 was fed into the cell and the NiO-YSZ anode was reduced into Ni-YSZ. Then, the reformate gas through methanol and ethanol steam reforming under the same conditions of catalytic tests was supplied to the Ni-YSZ anode, with a flow rate of 20 mL min^{-1}, while the LSCF-YSZ cathode was exposed to the ambient air. The open-circuit voltage was measured using an electrochemical test system at 700 °C. The performance stability was evaluated at 400 mA cm^{-2} and 700 °C with the reformate gas obtained by methanol steam reforming.

3. Results

3.1. Materials Characteristics

As shown in Figure 1a, both LBMNCu materials displayed a single perovskite phase like that of $LaMnO_3$ (PDF No. 35-1480) with no extra phase, indicating Ni and Cu elements were successfully inserted into the perovskite lattice. After reduction, the sample consisted of a primary phase of perovskite and a minor metallic phase at the peak around 44.5° and 52° corresponded to Ni-Cu alloy (PDF No. 65-7246), suggesting that metallic Ni-Cu particles were exsolved during reduction. The exsolution reaction for LBMNCu during reduction can be expressed as:

$$La_{0.8}Ba_{0.1}Mn_{0.8}Ni_{0.1}Cu_{0.1}O_3 + xH_2 = La_{0.8}Ba_{0.1}Mn_{0.8}Ni_{0.1-x/2}Cu_{0.1-x/2}O_{3-x} + x/2NiCu + xH_2O \quad (6)$$

where, x also represented the deficiency of O in the perovskite lattice. The maintenance of the perovskite structure also indicated that LBMNCu displayed good structural stability in the reducing atmosphere.

The corresponding specific surface area of the LBMNCu nanofibers (NFs) is 26 m^2 g^{-1}, larger than 11 m^2 g^{-1} of the LBMNCu nanoparticles (NPs) (Figure 1b), indicating the LBMNCu NFs possess a larger amount of active sites.

The LBMNCu materials via electrospinning method present the special morphology with characteristics of wrinkle-like nanofibers. Abundant hierarchical pores were exposed (Figure 2) due to the released gases from the decomposition and evaporation of PVP during the calcination process. Also, the wrinkled-like surface of nanofibers was changed to one consisting of interconnected particles, due to the exsolution of metallic nanoparticles after reduction, and the porous structures can clearly be observed. The special nanofiber structure could facilitate the adsorption of reactant and catalyze the formation and decomposition of H_2O. And the LBMNCu-NPs have a smooth surface without any impurity particles. After reduction, numerous metallic Ni-Cu NPs are observed, which are uniformly distributed throughout the reduced LBMNCu perovskite NF (R-LBMNCu-NF) surface. Fine metallic Ni-Cu NPs are also observed on the surface of the reduced LBMNCu perovskite NPs (R-LBMNCu-NPs), with an average size around 50 nm and uniform distribution, further proving the successful exsolution of Ni-Cu.

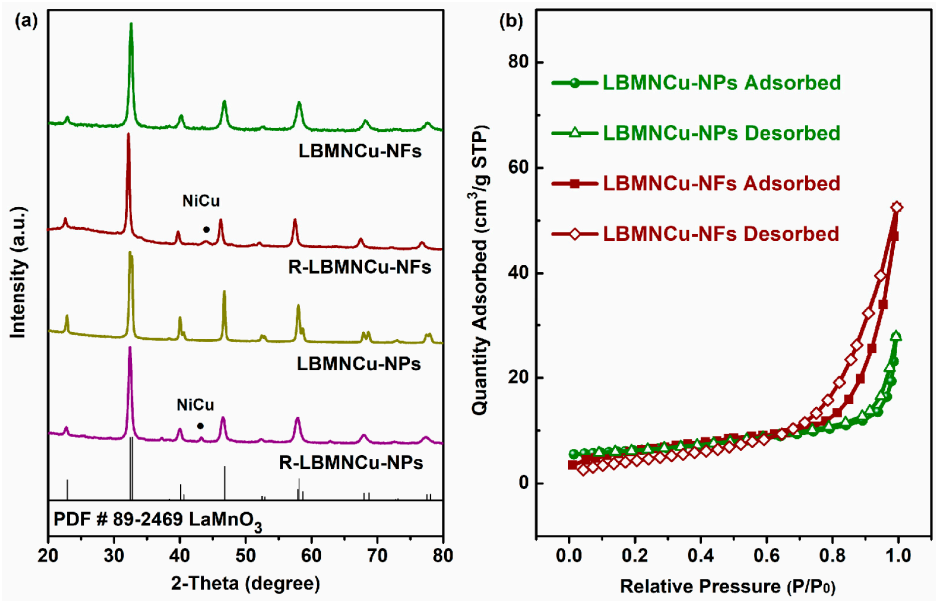

Figure 1. XRD patterns of as-prepared and reduced LBMNCu NF and NP catalysts. The samples were reduced in H_2 at 600 °C for 3 h (**a**). N_2 adsorption-desorption isotherms of LBMNCu NFs and NPs (**b**).

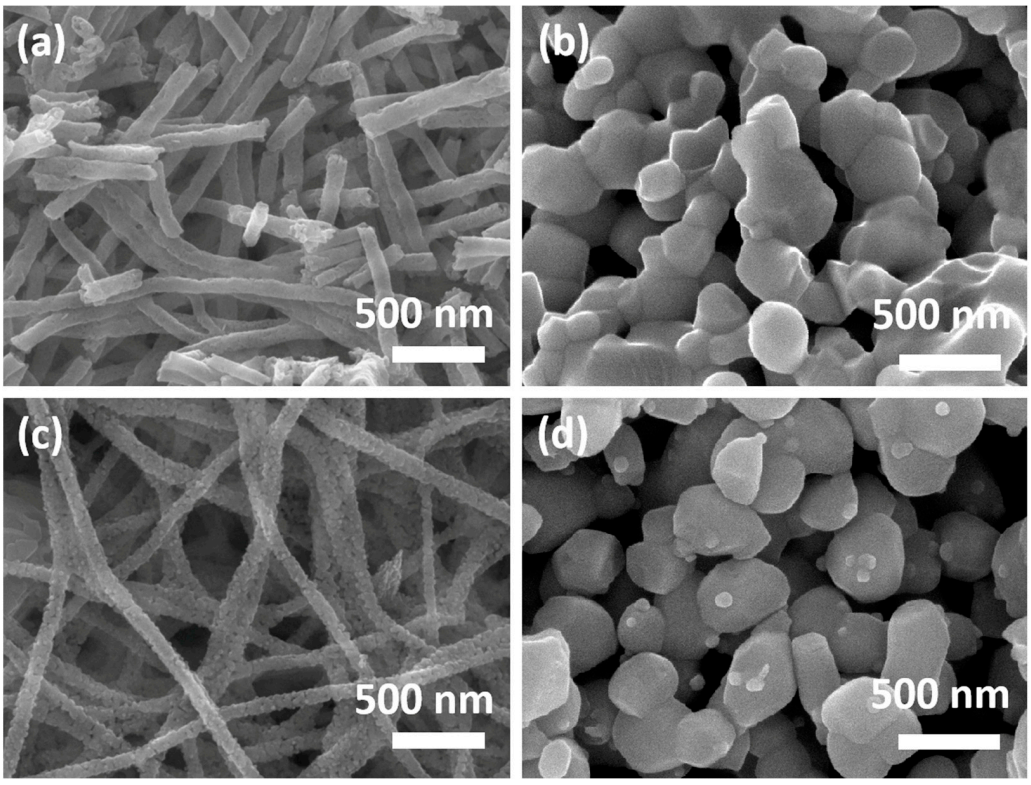

Figure 2. SEM images of as-prepared LBMNCu NFs (**a**), as-prepared LBMNCu NPs (**b**), and reduced LBMNCu NFs (**c**) and LBMNCu NPs (**d**).

3.2. MSR Test

When acting as a catalyst for MSR, the R-LBMNCu-NF catalysts, which were pre-reduced for 3 h, showed excellent activity in a methanol steam reforming test and the conversion increased with the increase of a water/methanol molar ratio (W/M) (Figure S1). Under the condition of 350 °C and 1.2 W/M ratio, the methanol conversion of R-LBMNCu-NFs was

above 80%, and the conversion was close to 90% at the 400 °C. When the temperature reached 450 °C, the reaction was nearly complete (Figure 3a). The methanol conversion of R-LBMNCu-NPs was lower than that of R-LBMNCu-NFs and better than that of Ni-Cu/Al_2O_3 under the same condition. Moreover, the CO concentration in the products for R-LBMNCu-NF catalysts was far less than that of the other two catalysts (Figure S2). According to the exhaust components analysis in the catalytic test, we can say the formation of CO was inhibited in our catalytic system and the concentration of CO in products was far below 0.01% at 450 °C, which suggested that the presence of Cu in the catalyst could effectively accelerate the water–gas shift reaction and suppress CO production.

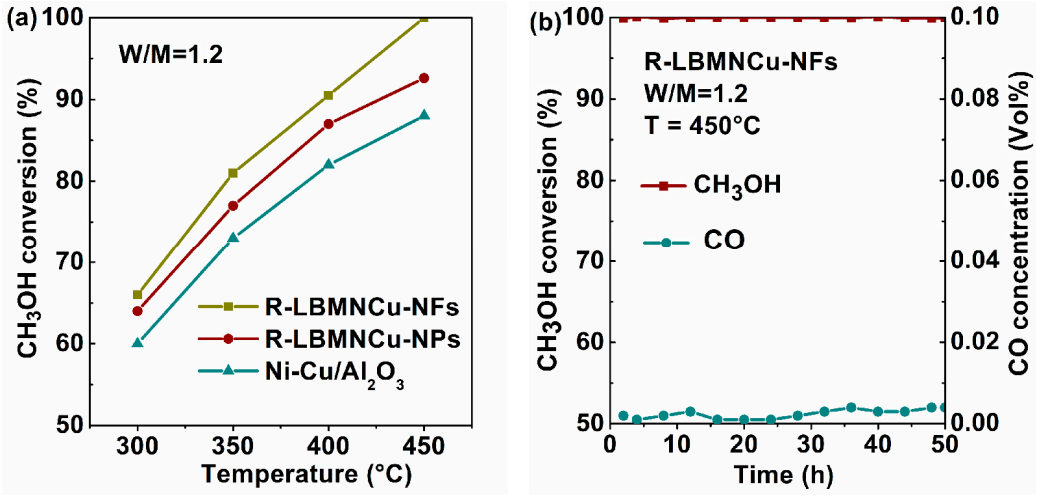

Figure 3. (**a**) The profiles of CH_3OH conversion of R-LBMNCu-NF, R-LBMNCu-NF and Ni-Cu/Al_2O_3 catalysts as a function of the reforming temperature with 1.2 W/M ratio. (**b**) CH_3OH conversion and CO molar concentration of R-LBMNCu-NF catalyst vs. time on stream for MSR reaction at 450 °C with a W/M ratio of 1.2.

The long-term stability of the R-LBMNCu-NF catalyst was tested at 450 °C with a W/M of 1.2. Similarly, the conversion rate of methanol stabilized above 99.9% and the CO concentration far below 0.01% within 50 h (Figure 3b). Meanwhile, the R-LBMNCu-NP catalyst displayed a degradation rate of 0.13% h^{-1} at 450 °C (from 92.4% to 85.9%) (Figure S3) and Ni-Cu/Al_2O_3 displayed a sharp decay rate of 0.46% h^{-1} (from 88% to 64.8%) (Figure S4). The slight attenuation of NPs and the highly stable catalytic properties of NFs indicate that the exsolution of metal nanoparticles is a good choice for MSR and R-LBMNCu-NF catalysts were highly efficient and suitable for methanol reforming for hydrogen production and further applications in solid oxide fuel cells.

3.3. ESR Test

For the R-LBMNCu-NF catalyst, the conversion of ethanol increased with the increase of temperature and a water/ethanol molar ratio (W/E) (Figure S5) and reached around 100% conversion of ethanol at 600 °C and W/E of 3.5 (Figure 4a). The R-LBMNCu-NP catalyst displayed a slightly lower conversion of 95% at 600 °C, which was also superior to the Ni-Cu/Al_2O_3 catalyst (Figure 4a). Moreover, the CO concentration in the products for R-LBMNCu-NF catalysts was far less than that of the other two catalysts (Figure S6), demonstrating that the presence of Cu in the catalyst could effectively suppress CO production during ESR and the optimum performance of R-LBMNCu-NF catalysts. It is noted that the W/E ratio did not considerably affect the amount of CO in the reformate gas, which was below 6% at 600 °C, suggesting that our catalytic system favors CO_2 formation (Figure S7).

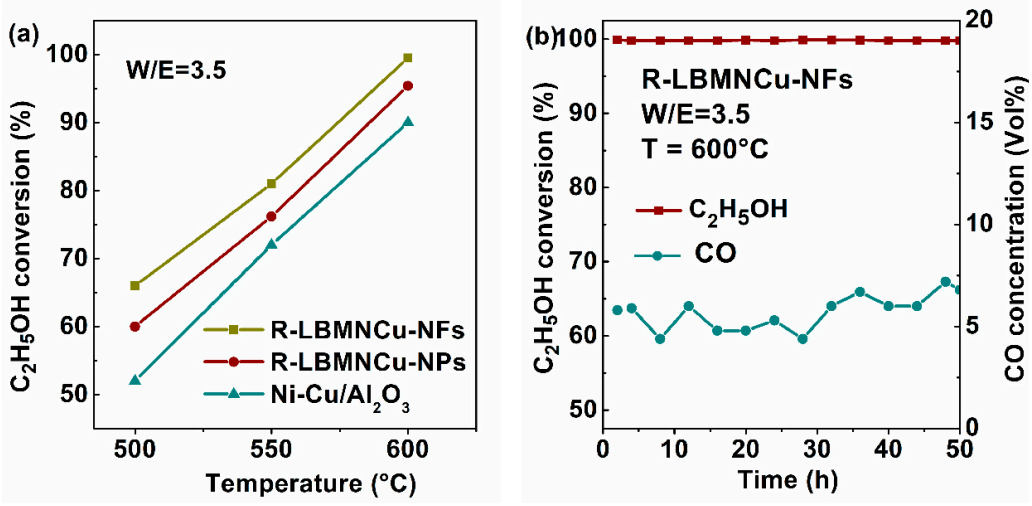

Figure 4. (**a**) The profiles of the C_2H_5OH conversion for R-LBMNCu-NF, R-LBMNCu-NP and Ni-Cu/Al_2O_3 catalysts as a function of the reforming temperature with 1.2 W/M ratio. (**b**) The profiles of C_2H_5OH conversion and CO molar concentration of the R-LBMNCu-NF catalyst during long-term test for ESR reaction at 600 °C and a W/E ratio of 3.5.

In a long-term test for the R-LBMNCu-NF catalyst, the conversion of ethanol reached 95% at 600 °C initially with a W/E ratio of 3 and then decreased gradually to 90% within 24 h, meanwhile the CO concentration slightly increased (Figure S8), which was possibly caused by carbon deposition, suggesting that more water needs to be added to maintain durability. At a W/E ratio of 3.5, ethanol conversion was maintained stably above 99.8% and CO concentration in the reformate gas below 10% for 50 h (Figure 4b). The highly stable catalytic performance of NFs further indicated that the exsolution of metallic nanoparticles was a good choice for ESR and R-LBMNCu-NF catalysts were highly efficient and suitable for methanol reforming for hydrogen production and further applications in solid oxide fuel cells.

3.4. Application

After the durability tests, the catalyst was examined and analyzed by Raman spectrometer, which is shown in Figure 5a. It was reported that the Raman peaks at 1350 cm^{-1} and 1580 cm^{-1} were related to typical carbon species (disordered carbon and graphitic carbon, respectively) [25]. After testing with methanol at 450 °C for 50 h with a 1.2 W/M ratio and ethanol at 600 °C with a W/E ratio of 3.5 for 50 h, no carbon peaks were observed by Raman spectrometry in the spent R-LBMNCu-NF catalyst, which resulted in a stable reforming performance. The microstructure of the R-LBMNCu-NF catalyst after MSR and ESR testing remained similar to the reduced ones (Figures 2c and 5b), without carbon deposition and obvious sintering, which also explained the catalytic stability.

After the above analysis, no carbon deposition was found for R-LBMNCu-NFs, which showed a good ability to resist carbon deposition and also indicated the CO formation was suppressed in the R-LBMNCu-NF system, so as to ensure the stability of reforming efficiency.

The cross-sectional morphology of the cathode, electrolyte and anode of the Ni–YSZ//YSZ//LSCF-YSZ SOFC single cell is shown in Figure 6a. The whole cell exhibited a distinct three layer structure and the LSCF-YSZ cathode was porous, with a thickness of about 25 m. The cathode was tightly connected to the YSZ electrolyte layer, and the thickness of YSZ electrolyte layer was about 10 μm, with good densification and no connected pores after sintering in air at 1390 °C for 4 h. The dense electrolyte blocks the contact between the fuel gas of the anode and the air of the cathode, ensuring the normal open circuit voltage. The Ni-YSZ anode had a porous structure, ensuring the transmission of fuel gas.

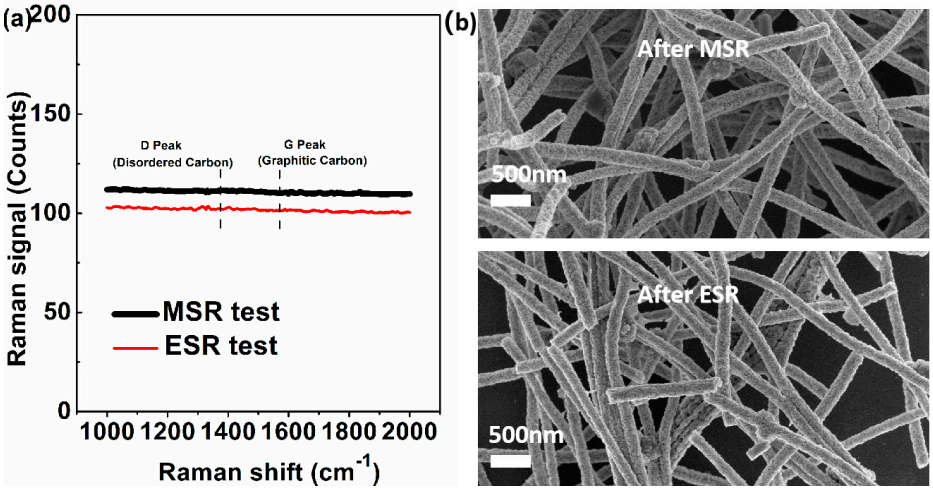

Figure 5. Raman spectrometry profiles of the R−LBMNCu−NF catalyst after testing with methanol at 450 °C for 50 h with a 1.2 W/M ratio and ethanol at 600 °C with a W/E ratio of 3.5 for 50 h (**a**), and the microstructure of the spent R-LBMNCu-NF catalyst (**b**).

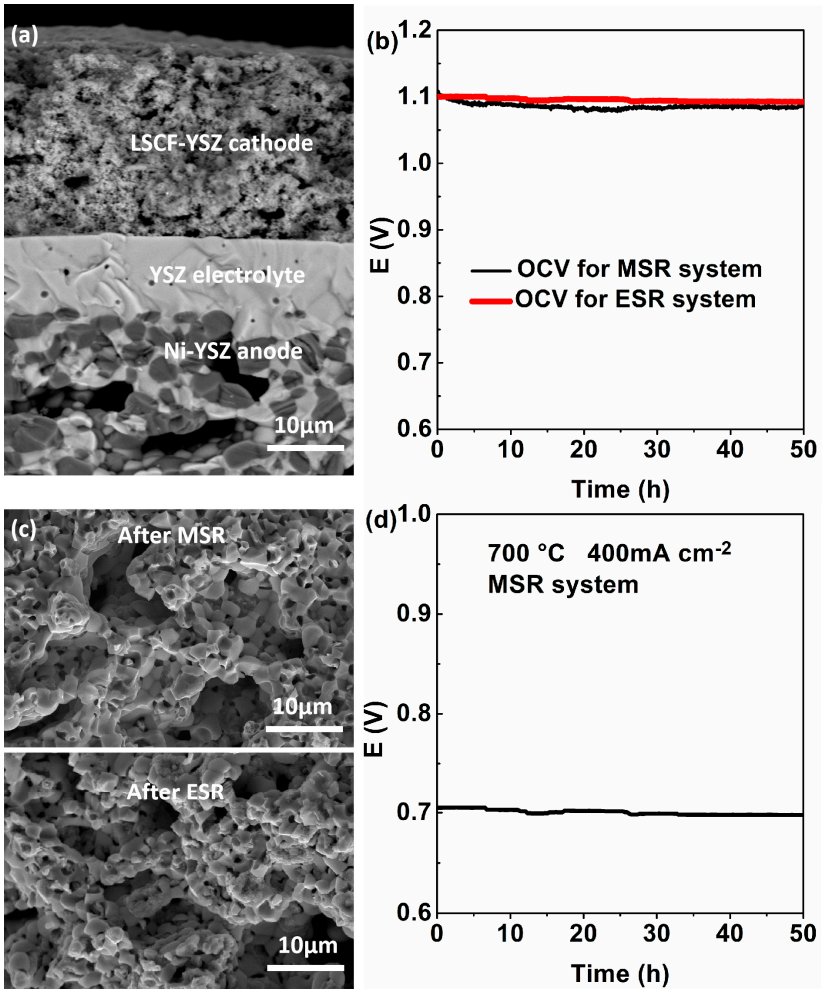

Figure 6. (**a**) Cross-sectional microstructure of SOFC with a triple-layer Ni−YSZ//YSZ//LSCF−YSZ structure. (**b**) The time-dependence of OCV of SOFC fueled by the reformate gas obtained by steam reforming methanol and ethanol under the same conditions of catalytic tests. (**c**) The microstructure of the Ni-YSZ anode exposed to reformed gas for 50 h. (**d**) Time-dependent cell voltage at 400 mA cm^{-2} with reformate gas obtained by methanol steam reforming at 700 °C.

Subsequently, the reformate gas through methanol and ethanol steam reforming under the same conditions of catalytic tests was fed in sequence into the anode of a single cell, at a flow rate of 20 mL min^{-1} for power generation at 700 °C. As shown in Figure 6a, the open-circuit voltage remained at a level of 1.1 V for 50 h without noticeable degradation (Figure 6b), and no carbon deposition or structure destruction was detected in the anode after external MSR or ESR (Figure 6c), demonstrating that the reformate gas via external steam reforming could not influence the microstructure and performance of SOFCs. The cells were also subjected to durability evaluation at galvanostatic discharge mode with the reformate gas obtained by methanol steam reforming. The voltage remained 0.7 V for 50 h (Figure 6d) at 700 °C and 400 mA cm^{-2}, which suggested the reformate gas could be considered as an ideal fuel for SOFCs to generate electric power.

4. Conclusions

In summary, a novel metal–ceramic composite catalyst with exsolved Ni dispersed on the perovskite substrate was introduced for MSR and ESR. The electrospinning method significantly increased the specific surface area of the catalysts and improved the catalytic performance. Ni nanoparticles can be exsolved from the substrate during the reduction in H_2 at 600 °C for 3 h. The obtained R-LBMNCu-NF catalyst displayed a methanol conversion rate near 100% when the temperature reached 450 °C at a 1.2 W/M ratio, and the conversion of ethanol reached around 100% at 600 °C with a W/E ratio of 3.5, which was superior to the general reforming catalyst Ni/Al_2O_3. In addition, during an electrochemical test, the open-circuit voltage of the single cell fueled by the reformate gas of MSR and ESR remained stable for up to 50 h without degradation and coking. In addition, the voltage remained at 0.7 V constantly for 50 h at 700 °C and 400 mA cm^{-2} during galvanostatic discharge mode. Thus, the reformate gas via the external steam reforming of alcohols can be considered as an effective fuel for SOFC power generation.

Supplementary Materials: The following supporting information can be downloaded at: https://www.mdpi.com/article/10.3390/cryst13111594/s1, Figure S1: CH_3OH conversion vs. temperature and W/M ratio for MSR reaction in the R-LBMNCu-NF catalyst system; Figure S2: Profiles of the CO molar concentration in gaseous products as a function of the reforming temperature with a 1.2 W/M ratio for R-LBMNCu-NF, R-LBMNCu-NF and Ni-Cu/Al_2O_3 catalysts; Figure S3: CH_3OH conversion and CO molar concentration of R-LBMNCu-NP catalysts vs. time on stream for MSR reaction at 450 °C with a W/M ratio of 1.2; Figure S4: CH_3OH conversion and CO molar concentration of Ni-Cu/Al_2O_3 catalysts vs. time on stream for MSR reaction at 450 °C with a W/M ratio of 1.2; Figure S5: C_2H_5OH conversion vs. temperature and W/E ratio for ESR reaction in the R-LBMNCu-NF catalyst system; Figure S6: Profiles of the CO molar concentration in the gaseous products of ESR as a function of the reforming temperature with a 3.5 W/E ratio for R-LBMNCu-NF, R-LBMNCu-NF and Ni-Cu/Al_2O_3 catalysts. Figure S7: Profiles of the CO molar concentration in the gaseous products as a function of the W/E ratio for ESR reaction in the R-LBMNCu-NF catalyst system. Figure S8: Profiles of C_2H_5OH conversion and CO molar concentration during long-term ESR test for R-LBMNCu-NF catalyst at 600 °C at a W/E ratio of 3.

Author Contributions: Conceptualization, T.W.; methodology, T.W.; validation, T.W. and J.W.; data curation, T.W. and Y.J.; formal analysis, Y.J.; software, T.W.; writing—original draft preparation, T.W.; writing—review and editing, T.W. and T.H.; project administration, T.H.; funding acquisition, T.W. and T.H. All authors have read and agreed to the published version of the manuscript.

Funding: This research was funded by the National Natural Science Foundation of China (52102316).

Data Availability Statement: The data presented in this study are available in the text and supplementary materials here.

Conflicts of Interest: The authors declare no conflict of interest.

References

1. Krishnakumar, T.; Kiruthiga, A.; Jozwiak, E.; Moulaee, K.; Neri, G. Development of ZnO-based sensors for fuel cell cars equipped with ethanol steam-reformer for on board hydrogen production. *Ceram. Int.* **2020**, *46*, 17076–17084. [CrossRef]
2. Shen, Q.; Jiang, Y.; Xia, F.; Wang, B.; Lv, X.; Ye, W.; Yang, G. Hydrogen production by Co-based bimetallic nano-catalysts and their performance in methane steam reforming. *Petrol. Sci. Technol.* **2020**, *38*, 618–625. [CrossRef]
3. Haryanto, A.; Fernando, S.; Murali, N.; Adhikari, S. Current status of hydrogen production techniques by steam reforming of ethanol: A review. *Energy Fuels* **2005**, *19*, 2098. [CrossRef]
4. Mateos-Pedrero, C.; Azenha, C.; DA, P.T.; Sousa, J.M.; Mendes, A. The influence of the support composition on the physicochemical and catalytic properties of Cu catalysts supported on Zirconia-Alumina for methanol steam reforming. *Appl. Catal. B-Environ.* **2020**, *277*, 119243. [CrossRef]
5. Li, H.; Tian, H.; Chen, S.; Sun, Z.; Liu, T.; Liu, R.; Assabumrungrat, S.; Saupsor, J.; Mu, R.; Pei, C.; et al. Sorption enhanced steam reforming of methanol for high-purity hydrogen production over Cu-MgO/Al_2O_3 bifunctional catalysts. *Appl. Catal. B-Environ.* **2020**, *276*, 119052. [CrossRef]
6. Pratihar, S.K.; Dassharma, A.; Maiti, H.S. Properties of Ni/YSZ porous cermets prepared by electroless coating technique for SOFC anode application. *J. Mater. Sci.* **2007**, *42*, 7220–7226. [CrossRef]
7. Hong, S.; Yang, H.; Lim, Y.; Prinz, F.B.; Kim, Y.-B. Grain-Controlled Gadolinia-Doped Ceria (GDC) Functional Layer for Interface Reaction Enhanced Low-Temperature Solid Oxide Fuel Cells. ACS Appl. *Mater. Interfaces* **2019**, *11*, 41338–41346. [CrossRef]
8. He, L.; Hu, S.; Jiang, L.; Liao, G.; Zhang, L.; Han, H.; Chen, X.; Wang, Y.; Xu, K.; Su, S.; et al. Co-production of hydrogen and carbon nanotubes from the decomposition/reforming of biomass- derived organics over Ni/α-Al_2O_3 catalyst: Performance of different compounds. *Fuel* **2017**, *210*, 307–314. [CrossRef]
9. Wu, C.; Williams, P.T. Hydrogen production from steam reforming of ethanol with nano-Ni/SiO_2 catalysts prepared at different Ni to citric acid ratios using a sol−gel method. *Appl. Catal. B-Environ.* **2011**, *102*, 251–259. [CrossRef]
10. Chang, C.C.; Chang, C.T.; Chiang, S.J.; Liaw, B.J.; Chen, Y.Z. Steam reforming of methanol over Cu/ZnO/CeO_2/ZrO_2/Al_2O_3 catalysts. *Appl. Catal. A-Gen.* **2009**, *358*, 7–12.
11. Yang, Q.; Zhou, C.; Ni, J.; Guan, X. Methane dry reforming in a coking- and sintering-free liquid alloy-salt catalytic system. *Sustain. Energy Fuels* **2020**, *4*, 2768–2774. [CrossRef]
12. Mateos-Pedrero, C.; Silva, H.; Tanaka, D.; Liguori, S.; Iulianelli, A.; Basile, A.; Mendes, A. CuO/ZnO catalysts for methanol steam reforming: The role of the support polarity ratio and surface area. *Appl. Catal. B-Environ.* **2015**, *174–175*, 67–76. [CrossRef]
13. Saracco, G.; Scibilia, G.; Iannibello, A. Methane Combustion on Mg-Doped $LaCrO_3$ Perovskite Catalysts. *Appl. Catal. B Environ.* **1996**, *8*, 229–244. [CrossRef]
14. Xu, X.; Su, C.; Shao, Z. Fundamental Understanding and Application of $Ba_{0.5}Sr_{0.5}Co_{0.8}Fe_{0.2}O_{3-\delta}$ Perovskite in Energy Storage and Conversion: Past, Present, and Future. *Energy Fuels* **2021**, *35*, 13585–13609. [CrossRef]
15. Rivas, I.; Alvarez, J.; Pietri, E.; Pérez-Zurita, M.; Goldwasser, M. Perovskite-type oxides in methane dry reforming: Effect of their incorporation into a mesoporous SBA-15 silica-host. *Catal. Today* **2010**, *149*, 388–393. [CrossRef]
16. Kwon, O.; Sengodan, S.; Kim, K.; Kim, G.; Jeong, H.Y.; Shin, J.; Ju, Y.W.; Han, J.W.; Kim, G. Exsolution trends and co-segregation aspects of self-grown catalyst nanoparticles in perovskites. *Nat. Commun.* **2017**, *8*, 15967. [CrossRef]
17. Nair, M.; Kaliaguine, S. Structured catalysts for dry reforming of methane. *New J. Chem.* **2016**, *40*, 4049–4060. [CrossRef]
18. Wei, T.; Jia, L.; Luo, J.-L.; Chi, B.; Pu, J.; Li, J. CO_2 dry reforming of CH_4 with Sr and Ni co-doped $LaCrO_3$ perovskite catalysts. *Appl. Surf. Sci.* **2019**, *506*, 144699. [CrossRef]
19. Neagu, D.; Oh, T.S.; Miller, D.N.; Ménard, H.; Bukhari, S.M.; Gamble, S.R.; Gorte, R.J.; Vohs, J.M.; Irvine, J.T. Nano- socketed nick el particles with en hanced coking r esistance grown in si tu by redox ex solution. *Nat. Commun.* **2015**, *6*, 8120. [CrossRef] [PubMed]
20. Neagu, D.; Tsekouras, G.; Miller, D.N.; Irvine, J.T. In situ growth of nanoparticles through control of non-stoichiometry. *Nat. Chem.* **2013**, *5*, 916–923. [CrossRef] [PubMed]
21. Jin, J.; Wu, L.; Huang, S.; Yan, M.; Wang, H.; Chen, L.; Hasan, T.; Li, Y.; Su, B. Hierarchy Design in Metal Oxides as Anodes for Advanced Lithium-Ion Batteries. *Small Methods* **2018**, *2*, 1800171. [CrossRef]
22. Xu, J.; Wang, Z.; Xu, D.; Meng, F.; Zhang, X. 3D ordered macroporous $LaFeO_3$ as efficient electrocatalyst for Li-O_2 batteries with enhanced rate capability and cyclic performance. *Energy Environ. Sci.* **2014**, *7*, 2213–2219. [CrossRef]
23. Wang, Z.; Zou, L.; Guo, S.; Sun, M.; Chen, Y.; Chi, B.; Pu, J.; Li, J. Porous double-doped perovskite $La_{0.6}Ca_{0.4}Fe_{0.8}Ni_{0.2}O_3$ nanotubes as highly efficient bifunctional catalysts for lithium-oxygen batteries. *J. Power Sources* **2020**, *468*, 228362. [CrossRef]
24. Zhang, X.; Gong, Y.; Li, S.; Sun, C. Porous perovskite $La_{0.6}Sr_{0.4}Co_{0.8}Mn_{0.2}O_3$ nanofibers loaded with RuO_2 nanosheets as an efficient and durable bifunctional catalyst for rechargeable Li-O_2 batteries. *ACS Catal.* **2017**, *7*, 7737–7747. [CrossRef]
25. Dresselhaus, M.; Dresselhaus, G.; Saito, R.; Jorio, A. Raman spectroscopy of carbon nanotubes. *Phys. Rep.* **2005**, *409*, 47–99. [CrossRef]